Organized Assemblies of Colloids Formed at the Poles of Micrometer-Sized Droplets of Liquid Crystal

Xiaoguang Wang,[a] Daniel S. Miller,[a] Juan J. de Pablo[b] and Nicholas L. Abbott[a,*]

[a] *Department of Chemical and Biological Engineering, University of Wisconsin-Madison, 1415 Engineering Drive, Madison, Wisconsin 53706-1607, USA. E-mail: abbott@engr.wisc.edu*

[b] Institute for Molecular Engineering, University of Chicago, 5801 South Ellis Avenue Chicago, Illinois 60637, USA.

Electronic Supplementary Information (ESI)

Distribution of positions of adsorbed polystyrene colloids between two boojums of the bipolar configuration of LC droplets

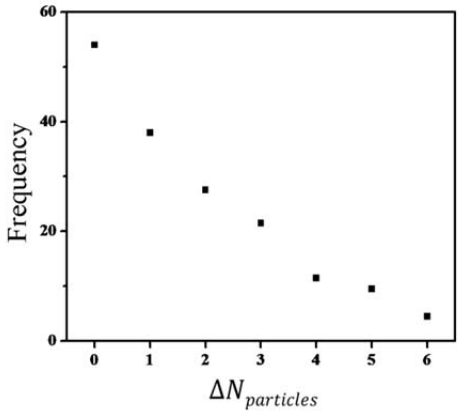

Fig. S1 Frequency with which different numbers of colloids were adsorbed to each of the two boojums of bipolar 5CB droplets.

Optical characterization of the anchoring of nematic 5CB on PS colloids adsorbed at planar aqueous—LC interface

As shown in Fig. S2, isolated PS colloids were observed to sediment onto LC films of nematic 5CB and create an optical signature with quadrupolar symmetry, consistent with the presence of two boojum defects at the surface of the colloid and elastic quadrupole—quadrupole interactions between PS colloids.[1-3]

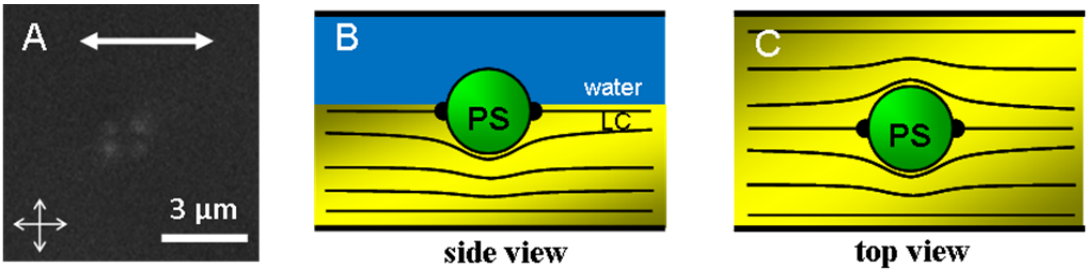

Fig. S2 (A) PL micrograph and schematic illustrations of a (B) side or (C) top view of a 1 µm-in-diameter PS colloid adsorbed at the planar aqueous interface of a 5CB film supported on a polyimide-coated glass slide. Double headed arrow in (A) indicates the rubbing direction of polyimide.

Enhancement of contrast in fluorescence images

In the main text, the contrast of raw Fluo images is enhanced to highlight the arrangements of colloids. A typical Fluo image after contrast enhancement is shown in Fig. S3A. The original image is shown in Fig. S3B. Comparison of the two micrographs reveals that the apparent spacing between the surfaces of the colloids is larger in raw images than enhanced images. All quantification of the spacing between colloids was performed using raw images.

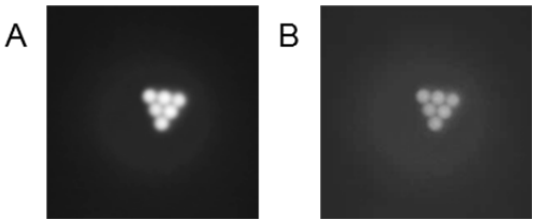

Fig. S3 Fluo micrograph of bipolar 5CB droplets with six colloids adsorbed at a pole (A) after and (B) before contrast enhancement. (A) is identical to that shown in Fig. 2 of the main text.

Spacing between PS colloids adsorbed at the surface of LC droplets in the presence of salt

We adsorbed PS colloids to the surfaces of 5CB droplets in the presence of 1 mM sodium chloride (NaCl). The center-to-center distance between adjacent colloids on LC droplets in the presence of NaCl was measured to be 1.07 ± 0.04 μm.

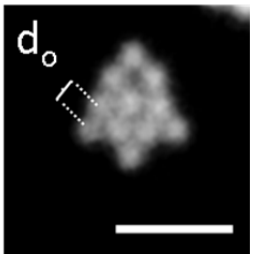

Fig. S4 Representative packing arrangements observed for 1 μm-in-diameter PS colloids adsorbed at a pole of nematic 5CB droplets in a bipolar configuration in the presence of 1 mM NaCl.

Role of nematic order in the formation of arrays of colloids adsorbed at the surface of LC droplets

We investigated the role of nematic order in the formation of the arrays of PS colloids by heating the LC droplets with colloids adsorbed into the isotropic phase. Fig. S4 shows representative Fluo micrographs of a LC droplet with three PS colloids adsorbed its surface before (Fig. S5A) and after (Fig. S5B) heating. The PS colloids were observed to dissociate from the initial hexagonal array and separate from one another on the surface upon heating the 5CB into the isotropic phase (we note here that the fluorescence signal of PS colloids decreased upon heating the 5CB into the isotropic phase because the dye is soluble in isotropic phase). Overall, the

above result leads us to conclude that the elastic energy of the strained LC drives the formation of hexagonal arrays of PS colloids at the poles of bipolar LC droplets.

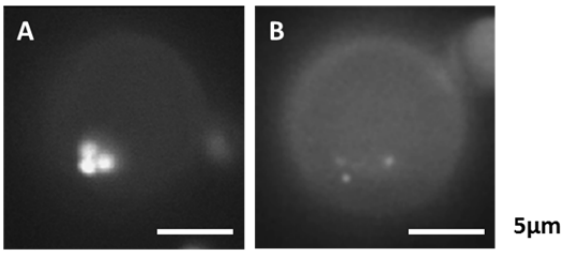

Fig. S5 Packing arrangements observed for PS colloids adsorbed at the surfaces of 5CB droplets (A) in nematic phase or (B) 30 s after heating into isotropic phase.

Derivation of the expression for splay attraction

Both in our previous studies[3-5] and the experiments reported in the main text, we observed colloids adsorbed at the surfaces of bipolar LC droplets to partition towards the surface defects to minimize the energetic penalty associated with high-splay distortion of the LC within these regions. Here we derive a simple order of magnitude estimate for this so-called "splay attraction" to the defects. We focus on a case in which one colloid is located at the center of a splay field where splay is at a maximum, and a second colloid subsequently introduced into the field is also attracted to this location (Fig. S6).

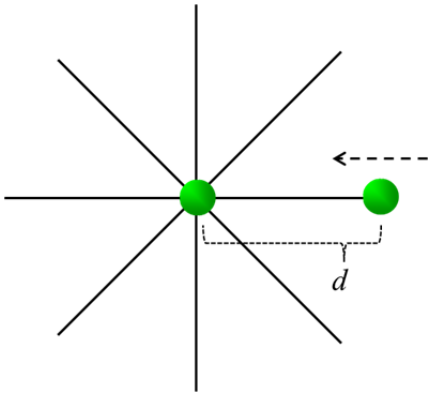

Fig. S6 Schematic illustration of splay attraction. First, a single colloid is placed at the region of maximum splay. A second colloid introduced into the field is attracted towards this high-splay region.

The elastic energy density of the splay field can be estimated from the splay term in the Frank–Oseen equation[6]:

$$f_e = \frac{1}{2}[K(\nabla \cdot \bar{n})^2] \quad \text{(S1)}$$

in which K is the splay elastic constant, and $\bar{n}$ is a vector of order unity that represents the local orientation of the LC (the so-called nematic director). In spherical coordinates $\nabla \cdot \bar{n} = \frac{1}{r^2}\frac{d}{dr}(r^2 n_r)$. Thus, eqn S1 scales as:

$$f_e = \frac{2K}{d^2} \quad \text{(S2)}$$

in which d is distance of a colloid from the boojum defect occupied by another colloid (Fig. S6). From eqn S2 we estimate the splay attraction energy as:

$$E_{splay} = -\left(\frac{4}{3}\pi a^3\right)\left(\frac{2K}{d^2}\right) = -\frac{8}{3}\pi K\frac{a^3}{d^2} \quad \text{(S3)}$$

in which a and $\frac{4}{3}\pi a^3$ are the radius and volume of a PS colloid, respectively. Eqn S3 predicts the energy gain as a function of the position of the second colloid (d). The smallest d is the experimentally observed center-to-center spacing between PS colloids in the vicinity of the boojum defect. Eqn S3 is eqn 1 of the main text.

Contact angle for PS colloids adsorbed at the surfaces of LC droplets

We used 4 μm-in-diameter PS colloids to measure the contact angle for PS colloids adsorbed at the aqueous—LC interface of a LC droplet, as shown in Fig. S7. 4 μm-in-diameter PS colloids were used so that the colloids could be resolved in bright field micrographs (instead of 1 μm-in-diameter). The contact angle is measured to be ~ 95°.

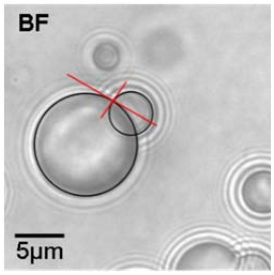

Fig. S7 Contact angle for a 4 μm-in-diameter PS colloid adsorbed at the surface of nematic LC droplet. The contact angle is measured to be ~ 95°.

Measurement of surface charge density of PS colloids

The surface charge density of PS colloids was calculated from zeta-potential measurements using the following equation:

$$\sigma = \frac{2\varepsilon_0\varepsilon_w\kappa kT}{ze}\sinh\left(\frac{ze\zeta}{2kT}\right)\left[1+\frac{1}{\kappa a}\frac{1}{\left(\cosh\frac{ze\zeta}{4kT}\right)^2}\right] \quad \text{(S4)}$$

in which σ is surface charge density, ε_0 is the permittivity of vacuum (8.85x10^{-12} C^2/J·m), ε_w is dielectric constant of water (78) , κ is Debye-Huckel parameter ($1/\kappa$ is Debye screening length), k is the Boltzmann constant, T is the temperature, z is the valence number, e is the electronic charge, ζ is the zeta potential, and a is the radius of PS colloid (0.5 μm).[7] κ can be calculated as:

$$\kappa = \left(\frac{e^2 \sum_i c_i z_i^2}{\varepsilon_0 \varepsilon_w kT}\right)^{\frac{1}{2}} \quad \text{(S4)}$$

in which c is the concentration of ions per m^3. The results are summarized in Table S1. The average charge density is calculated to be 0.06 e$^-$/nm^2.[7]

Table S1 Calculation of apparent surface charge density on PS colloids based on zeta-potential measurement.

zeta potential (mV)	salt concentration (mM)	Debye length (nm)	surface charge density (e$^-$/nm^2)
-5.8	1000	0.30	0.08
-11.7	100	0.96	0.05
-15.1	75	1.11	0.06
-18.7	50	1.36	0.06

Analysis of the relative stabilities of packing arrangements of five PS colloids on the surfaces of bipolar LC droplets

We analyzed the frequency distributions of the packing arrangements shown in Figure 2 under the assumption that they corresponded to equilibrium states of the systems. Under this assumption, the relative energies of the packing arrangements can be calculated from the frequency distribution (Fig. 4 of the main text) using a Boltzmann distribution ($F(N) \propto M(N)e^{-E(N)}$; where M and E are the multiplicity of arrangements and energy (in units of k_BT) for a given N, respectively). Therefore, we plot $-\ln(F/M)$ as a function of N in Fig. S8. The

analysis predicts that the energy of the system is lowered by increasing N within an arrangement of five colloids (a line fit to the data predicts an energy gain of ~0.8 k_BT per N), and that $N = 7$ is the energetically most stable arrangement. However, we note that the difference in energy between arrangements of different N is small (of order k_BT). This conclusion is not consistent with our observation that the arrangements were "frozen" over periods of hours (if the intercolloid interactions were of order kT, thermal fluctuations would lead to rearrangements of the colloids). We thus conclude that the frequency distribution obtained from our experimental observation is likely influenced by kinetic barriers that prevent rearrangement and that assemblies of five colloids with $N < 7$ are kinetically trapped states.

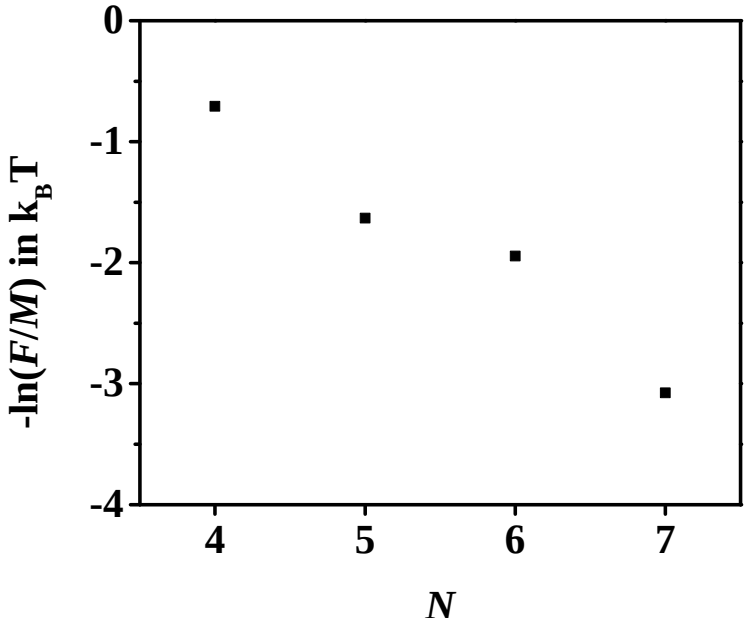

Fig. S8 Negative natural logarithm of F/M (in units of k_BT) plotted as function of N. The plots were constructed from Fig. 2 of the main text.

References

1. H. Stark, *Physics Reports*, 2001, **351**, 387-474.
2. P. Poulin and D. Weitz, *Physical Review E*, 1998, **57**, 626.
3. F. Mondiot, X. Wang, J. J. de Pablo and N. L. Abbott, *Journal of the American Chemical Society*, 2013, **135**, 9972–9975.
4. J. K. Whitmer, X. Wang, F. Mondiot, D. S. Miller, N. L. Abbott and J. J. d. Pablo, *Physical Review Letters*, 2013, **111**, 227801.
5. X. Wang, D. S. Miller, J. J. d. Pablo and N. L. Abbott, *Advanced Functional Materials*, 2014 (In Press).
6. F. C. Frank, *Discussions of the Faraday Society*, 1958, **25**, 19-28.
7. K. Makino and H. Ohshima, *Langmuir*, 2010, **26**, 18016-18019.